J. Fluid Mech. (2004), *vol.* 515, *pp.* 353–370.
DOI: 10.1017/S002211200400045X Printed in the United Kingdom

Fibre coating: non-unique solutions at small capillary numbers

By P. A. BLYTHE[1] AND P. G. SIMPKINS[2]†

[1]Department of Mechanical Engineering & Mechanics, Lehigh University, Bethlehem, PA 18015, USA
[2]Optical Fiber Research, Bell Laboratories, Murray Hill, NJ 07974, USA

(Received 5 June 2000 and in revised form 12 May 2004)

Lubrication theory is employed to examine surface-tension-dominated flows that arise during the application of thin coatings, using pressurized dies, to axially symmetric fibres. In all cases, it is assumed that the clearance between the die exit and the fibre is small compared with the fibre diameter. Previous analyses have been concerned with flows controlled by axial curvature for which the resulting solutions are unique. The present investigation examines stationary flows in which both the axial and the azimuthal curvatures are comparable. It is shown that this situation develops when the applicator volume flow is sufficiently large. Moreover, as the volume flow is increased, spatially oscillatory menisci can exist such that the solution is not always unique. These results are new, and calculations are presented that determine the maximum die clearance below which the solution remains unique. Within this regime, surface oscillations do not occur and there is a monotonic decay to the final uniform coating thickness.

1. Introduction

Surface-tension-dominated flows play an important role in numerous coating techniques. Typical examples are found in offset printing, fibre spinning, microelectronics and physiology. In particular, protective coatings of extreme precision are required for magnetic tapes, CD-ROM surfaces and optical fibres. Reviews have been given by de Gennes (1985), Ruschak (1985), Benjamin & Scriven (1991), Myers (1998) and Quéré (1999). Stability analyses for related free-surface flows have been discussed by Eggers (1997), and a comprehensive survey of the dynamics of thin liquid films can be found in Oron, Davis & Bankoff (1997). Current difficulties associated with ultrathin coatings, including spinodal dewetting, are described in Weiss (1999). Some of the examples noted above are associated with plane geometries, but axially symmetric flows that arise in the coating of thin filaments present additional challenges.

This paper is concerned with flows that develop in the coating of fibres using pressurized applicators or dies. In this process, a fibre is pulled through a shaped die at a specified speed, and the geometry and the supply pressure are selected to produce the required coating thickness. Equivalently, the die generates the necessary applicator volume flow. After passage through the applicator, the coating is cured to enhance solidification. Prior to curing, it is important that the coating has reached its final asymptotic thickness in a monotonic manner. Clearly, curing must take place

† Present address: College of Engineering & Computer Science, Syracuse University, Syracuse, NY 12344, USA.

before the growth of any temporal instabilities that are inherent in this type of coating process (Quéré 1999). All flows considered here are assumed to be time-independent and axially symmetric.

Landau & Levich (1942) used lubrication theory to analyse planar free surface shapes for surface-tension controlled flows at small capillary numbers Ca. Their analysis is also relevant to certain non-planar applications including the behaviour of thin annular films in long tubes, some aspects of fibre coating, etc. (Bretherton 1961; Middleman 1995; Jensen 1997). In these flows, axial curvature dominates and the results are valid in the limit when the dimensionless volume flow $Q = \delta = O(Ca^{2/3})$, where δ is the ratio of the final coating thickness to the fibre radius. At larger volume flows, both curvature terms become important, and the Landau–Levich approach is no longer valid. Specifically, this occurs when $Q = \delta = O(Ca^{1/3})$, and the related flow structure is outlined in the present paper. It is shown that the free-surface shape is now controlled by a modified capillary number $\lambda = 3\,Ca\delta^{-3}$. The Landau–Levich equation can be recovered in the limit $\lambda \to \infty$.

Related analyses for unsteady flows have been given by Hammond (1983), Frenkel (1992) and Kalliadasis & Chang (1994). In each case, they developed suitable nonlinear evolution equations for axially symmetric disturbances. Frenkel used such an equation to discuss film break-up on vertical cylinders, and observed that the theory was consistent with existing experimental data (Quéré 1990; see also de Ryck & Quéré 1996). An equivalent equation was considered by Kalliadasis & Chang who examined the propagation of solitary waves on thin films of unbounded extent in the axial direction. Unsteady thin-film flows are also discussed in the review papers by Oron *et al.* and Myers. By choosing appropriate frames of reference, subject to suitable asymptotic limits, it can be shown that these wave equations reduce to the nonlinear steady form analysed in the present paper. An earlier formulation of the steady equation was noted in Blythe & Simpkins (1995). More recently, the equation was also derived in an analysis of dip-coating processes (Darhuber *et al.* 2000).

In contrast with the Kalliadasis–Chang approach, the current analysis is concerned with stationary solutions for a semi-infinite fibre when the meniscus is pinned at the exit of a coating applicator. Calculations indicate that, if the die clearance (or equivalently the volume flow) is sufficiently large, a steady spatial oscillation develops on the free surface. The solutions are analogous to those obtained for the Laplace–Young equation in analyses of pendant drops (see Finn 1986). Because the governing differential equation is translationally invariant in the axial direction, it follows that above a certain (critical) die clearance the meniscus profile is not always uniquely defined when the free surface is oscillatory. Determination of the critical die clearance, as a function of the controlling parameter λ, is important in die design. These steady semi-infinite problems do not appear to have been considered previously, and this paper provides a mathematical description of low-capillary-number flows that contain spatial oscillations. Physically, the existence of these flows is controlled by their stability. Detailed stability considerations are beyond the scope of the present study, but elementary arguments suggest, and practical experience demonstrates, that curing processes restrict the growth of certain spatio-temporal oscillations.

Appropriate dimensionless forms of the governing equations, based on the lubrication limit, are set out in § 2. In § 3 the basic solution for the velocity distribution in the free surface region is determined. A review of the small-gap Landau–Levich theory, with $Q = O(Ca^{2/3})$, is given in § 4. Extension to larger gaps, with $Q = O(Ca^{1/3})$, is outlined in § 5. Non-unique solutions are discussed in § 6, as is the evaluation of the critical gap size. Verification of the computational results for the critical gap is carried

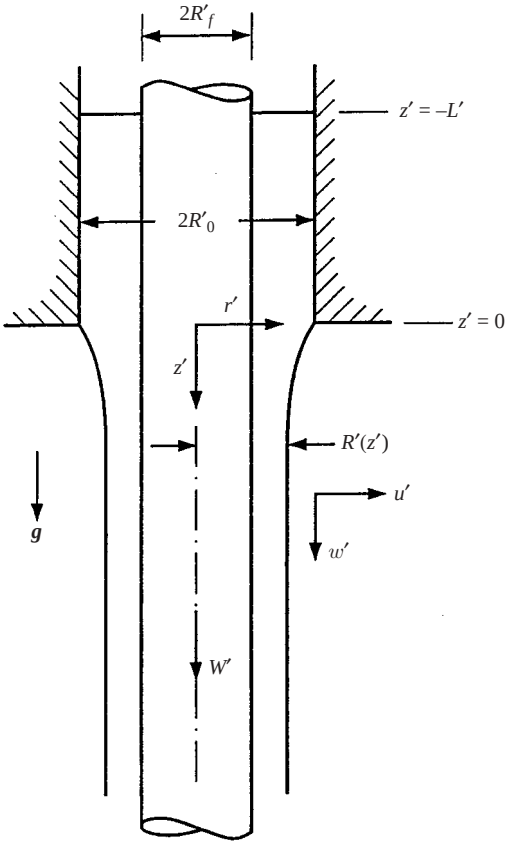

FIGURE 1. Geometry and coordinate system in dimensional units.

out by considering an intermediate asymptotic analysis with $\lambda \gg 1$ or, equivalently, with $Ca^{1/3} \gg Q \gg Ca^{2/3}$. Comparisons with the numerical calculations are made in § 7; excellent agreement is found. Application of the approach to a cylindrical die is described in § 8, together with calculations of the volume flow–pressure gradient relationship (Middleman 1998). Stability issues and the associated time scales are briefly examined in § 9.

2. Governing equations

In the die-coating process considered here, an incompressible Newtonian fluid with constant properties is withdrawn from an axisymmetric applicator bath of depth L' by a fibre of radius R'_f moving vertically downwards at a speed W'. The basic free-surface flow is shown in figure 1. No detailed assumptions about the applicator shape are made in the general analysis given below. For thin coatings, suitable dimensionless radial and axial coordinates are defined by

$$r' = R'_f(1 + \delta s), \quad z' = R'_f z, \tag{2.1}$$

with $s = 0$ on the fibre surface; here $\delta \ll 1$ is the dimensionless asymptotic coating thickness. On the free surface

$$r' = R'_f(1 + \delta h) \quad \text{or} \quad s = h(z), \tag{2.2}$$

so that, from the definition of δ,

$$h \to 1 \quad \text{as} \quad z \to \infty. \tag{2.3}$$

Corresponding dimensionless velocity components in the radial and axial directions, respectively, are

$$(u', w') = W'(\delta u, w), \tag{2.4}$$

and conditions at the fibre surface require that

$$(u, w) = (0, 1) \quad \text{on} \quad s = 0. \tag{2.5}$$

In addition, the kinematic condition at the free surface demands that

$$u = w\frac{\mathrm{d}h}{\mathrm{d}z} \quad \text{on} \quad s = h. \tag{2.6}$$

This paper is concerned with surface-tension-dominated flows in which both axial and azimuthal curvature effects are important. It is assumed throughout that the capillary number

$$Ca = \frac{\mu W'}{\sigma} \ll 1, \tag{2.7}$$

where μ is the viscosity and σ is the surface tension. Pressures are measured relative to the ambient external value including the constant contribution from the unperturbed azimuthal curvature $R_f'^{-1}$. An appropriate dimensionless pressure difference p is then defined by

$$\Delta p' = \delta\frac{\sigma}{R_f'}p. \tag{2.8}$$

From the usual normal stress balance at the free surface (see e.g. Batchelor 1967), it follows that

$$p = -h - \frac{\mathrm{d}^2h}{\mathrm{d}z^2} \quad \text{on} \quad s = h, \tag{2.9}$$

where terms $O(\delta, \delta^{-1}Ca)$, have been neglected. For the basic limit discussed in this paper, see (2.11) below, $Ca = O(\delta^3)$ and the dominant error in (2.9) is $O(\delta)$. In (2.9), $-h$ and $-\mathrm{d}^2h/\mathrm{d}z^2$ represent the local approximations to the principal curvatures, see Hammond (1983). (Only $\mathrm{d}^2h/\mathrm{d}z^2$ occurs in the planar case.) Neglecting terms $O(\delta^2)$, the tangential stress balance at the free surface gives

$$\frac{\partial w}{\partial s} = 0 \quad \text{on} \quad s = h. \tag{2.10}$$

For the thin-film limit $\delta \ll 1$ with $\delta Re = o(1)$, where the Reynolds number Re is based on the asymptotic coating thickness, the axial momentum equation implies that there is a balance between the pressure gradient and the viscous terms for $Ca = O(\delta^3)$. In this case the inertial terms, of relative size δRe, can be neglected. With

$$\lambda = 3\frac{Ca}{\delta^3} = O(1), \tag{2.11}$$

where the factor 3 has been inserted for later algebraic convenience, the leading approximation to the Navier–Stokes equations is the conventional lubrication limit

(see e.g. Middleman 1995),

$$\frac{\partial u}{\partial s} + \frac{\partial w}{\partial z} = 0, \tag{2.12}$$

$$-3\lambda^{-1}\frac{\partial p}{\partial z} + \frac{\partial^2 w}{\partial s^2} = 0, \tag{2.13}$$

$$\frac{\partial p}{\partial s} = 0. \tag{2.14}$$

Here, terms $O(\delta Re, \delta)$ and smaller have been neglected In (2.13), the body-force contribution has also been ignored; this factor is usually extremely small in fibre-coating applications.

3. Free-surface evolution

From (2.5), (2.9), (2.10), (2.13) and (2.14) it follows that

$$w = 1 - K(z)\left[h(z)s - \tfrac{1}{2}s^2\right], \tag{3.1}$$

with

$$K(z) = \frac{3}{\lambda}\frac{\mathrm{d}p}{\mathrm{d}z} = -\frac{3}{\lambda}\left(\frac{\mathrm{d}h}{dz} + \frac{\mathrm{d}^3 h}{\mathrm{d}z^3}\right). \tag{3.2}$$

For stationary flows the dimensionless volume flux Q is constant, and from (3.1) is given by

$$Q = \delta\int_0^h w\,\mathrm{d}s = \delta\left(h - \tfrac{1}{3}Kh^3\right). \tag{3.3}$$

As $z \to \infty, h \to 1$ and $K \to 0$, so that from (3.3)

$$Q = \delta. \tag{3.4}$$

An alternative expression for Q can be deduced from the applicator flow field, which depends on the geometry and on the applied pressure gradient. This relationship is given in § 8 for a simple cylindrical applicator. The result enables δ to be found for a given exit gap and pressure gradient. It should be emphasized that no specific choice for the applicator geometry is required in the general analysis presented below. From (3.2)–(3.4), the free-surface shape is governed by

$$h^3\left(\frac{\mathrm{d}^3 h}{\mathrm{d}z^3} + \frac{\mathrm{d}h}{\mathrm{d}z}\right) = -\lambda(h-1), \tag{3.5}$$

which must be solved subject to (2.3) and an initial condition

$$h = h_i \quad \text{at} \quad z = 0. \tag{3.6}$$

The steady equation (3.5) was derived in Blythe & Simpkins (1995), and an application to dip-coating phenomena can be found in Darhuber *et al.* (2000). Experimental results given in Darhuber *et al.* confirm the scaling law defined by (2.11) and (3.5).

4. The Landau–Levich limit

For large modified capillary numbers, i.e. $\lambda \gg 1$, the seminal Landau & Levich description can be recovered in the limit $\delta = Q = O(Ca^{2/3})$. An appropriate

independent variable is

$$y = z\lambda^{1/3} \quad \text{or} \quad z = y\delta^{1/2}\left(\frac{3Ca}{\delta^{3/2}}\right)^{-1/3}. \tag{4.1}$$

Consequently, for $\delta = O(Ca^{2/3})$, $z = O(\delta^{1/2})$. In this limit, axial curvature dominates with $\delta \mathrm{d}^2h/\mathrm{d}z^2 = O(1)$, and $u = O(\delta^{-1/2})$. It follows from (3.5) that

$$h^3\frac{\mathrm{d}^3h}{\mathrm{d}y^3} = 1 - h, \tag{4.2}$$

see Bretherton (1961). This result can also be deduced more generally for $\delta = o(Ca^{1/3})$ by writing

$$\delta = \Delta(3Ca)^{1/3}, \quad z = \Delta y, \quad \Delta = o(1). \tag{4.3}$$

Properties of (4.2) and related equations are discussed in Tuck & Schwartz (1990). For the choice $h_i = 2$, the numerical solution of (4.2), using (2.9), yields

$$p_e = (p)_{z=0} = -\frac{1}{\delta}\left(\frac{3Ca}{\delta^{3/2}}\right)^{2/3}\left(\frac{\mathrm{d}^2h}{\mathrm{d}y^2}\right)_{y=0} = -\lambda^{2/3}\left(\frac{\mathrm{d}^2h}{\mathrm{d}y^2}\right)_{y=0} \quad \text{with} \quad \left(\frac{\mathrm{d}^2h}{\mathrm{d}y^2}\right)_{y=0} \approx 0.4229 \tag{4.4}$$

as the dominant approximation to the applicator exit pressure. This initial gap corresponds to the unpressurized applicator considered in § 8 (see Batchelor 1967; Middleman 1998). A comparison with results for the full equation (3.5) is discussed in § 5.

5. Larger gaps

For thin films, the distinguished limit defined by (3.5) with $\lambda = O(1)$ occurs when $\delta = Q = O(Ca^{1/3})$. Although these flows arise for significantly larger exit gaps than those discussed in § 4, where $\delta = O(\Delta Ca^{1/3})$, the die clearance is still small compared with the fibre radius. For $\lambda = O(1)$, h is again required to satisfy the initial and asymptotic conditions listed in (3.6) and (2.3). As shown in Appendix A, satisfaction of (2.3) imposes two constraints on (3.5) and implies that the asymptotic decay ($z \to \infty$) towards $h = 1$ is monotonic. Numerical solutions of (3.5), subject to (3.6) and (2.3), can be found using the technique described in Appendix B. Solution profiles with $h_i = 2$ are shown in figure 2 for various λ.

It was observed in § 4 that the Landau–Levich equation (4.2) can be obtained from (3.5) in the limit $\lambda \to \infty$ at fixed h_i. A comparison between (4.2) and (3.5) is made in figure 2 for the particular case $\lambda = 5$. Note that the z and y scales are related by (4.1). Even at this modest value of λ, the solutions are in good agreement.

The corresponding limiting solution as $\lambda \to 0$, with h_i fixed, is also easily obtained. Inspection of (3.5) suggests the scaling

$$z = \lambda^{-1}\xi \quad \text{with} \quad h = N_0(\xi) + \lambda^2 N_1(\xi) + \ldots. \tag{5.1}$$

Hence,

$$\frac{\mathrm{d}N_0}{\mathrm{d}\xi} = -\frac{N_0 - 1}{N_0^3}, \tag{5.2}$$

so that

$$\xi = g(h_i) - g(N_0), \tag{5.3}$$

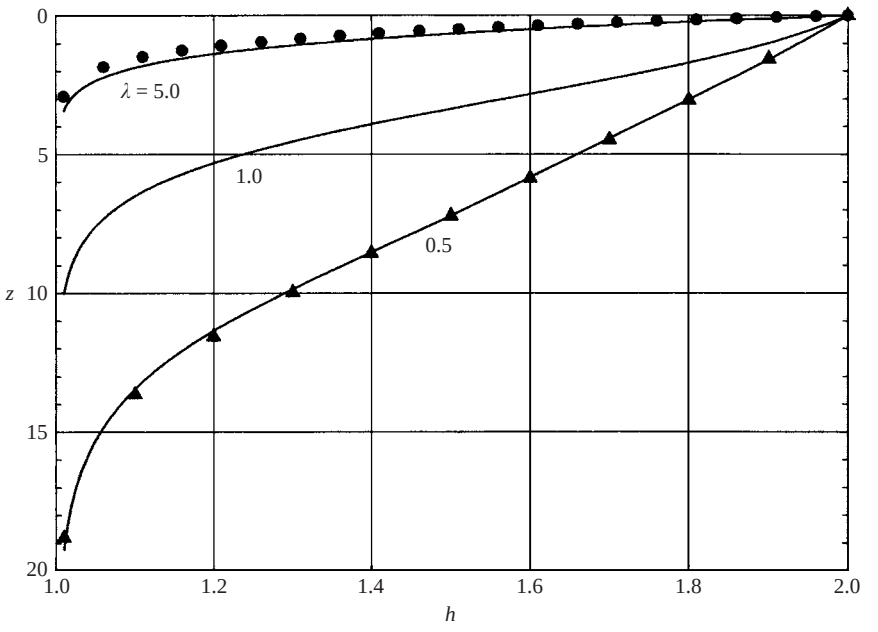

FIGURE 2. Free-surface profiles for $h_i = 2.0$: unique solutions. Also shown are ●, the Landau–Levich result for $\lambda = 5.0$, and ▲, the small λ result (5.3) for $\lambda = 0.5$.

where

$$g(h) = \tfrac{1}{3}(h-1)^3 + \tfrac{3}{2}(h-1)^2 + 3(h-1) + \ln(h-1). \tag{5.4}$$

The result (5.4) defines a universal profile in which the endpoint, see (5.3), is defined by the choice of h_i. This solution, for which the z and ξ scales are connected by (5.1), is also displayed in figure 2 for the particular case $\lambda = 0.5$. Even at this value of λ, the agreement with the full equation (3.5) is remarkably good.

For each of the cases shown in figure 2, the coating thickness decays monotonically to its asymptotic value ($h = 1$) as $z \to \infty$. At larger values of h_i, this monotonic behaviour does not persist for all λ. As noted in Appendix B, by introducing

$$\bar{z} = z_0 - z \tag{5.5}$$

the results, for a given λ, can be obtained for various h_i by backward integration of (3.5) starting from the asymptotic state

$$h = 1 + \bar{h}_b \quad \text{at} \quad \bar{z} = 0 \quad \text{with} \quad 0 < \bar{h}_b \ll 1. \tag{5.6}$$

The spatial location $z = 0$ is identified by the point ($\bar{z} = z_0$) at which h_i attains the required value. Typical results for $\lambda = 1.5$, 2.0 and 2.5, using the same starting value for $\bar{h}_b$, are displayed in figure 3. With an initial gap $h_i = 2.75$, the solutions remain monotonic for $\lambda = 1.5$ and 2.5, although the sign of the curvature changes. When $\lambda = 2.0$, there is an oscillation in the coating thickness prior to attaining $h_i = 2.75$.

All solutions shown in figure 3 for $h_i = 2.75$ are unique. Continuation of the integration at $\lambda = 2$, however, yields the result shown in figure 3. From this figure, it is apparent that there is only one $\bar{z}$-location at which $h = 2.75$, although this is obviously not true for all choices of h_i. In particular, when $h_i = 3.5$ there are three such locations and the solution is therefore not unique. (Because (3.5) is invariant under translation in z, each of these locations can serve as the initial station at which

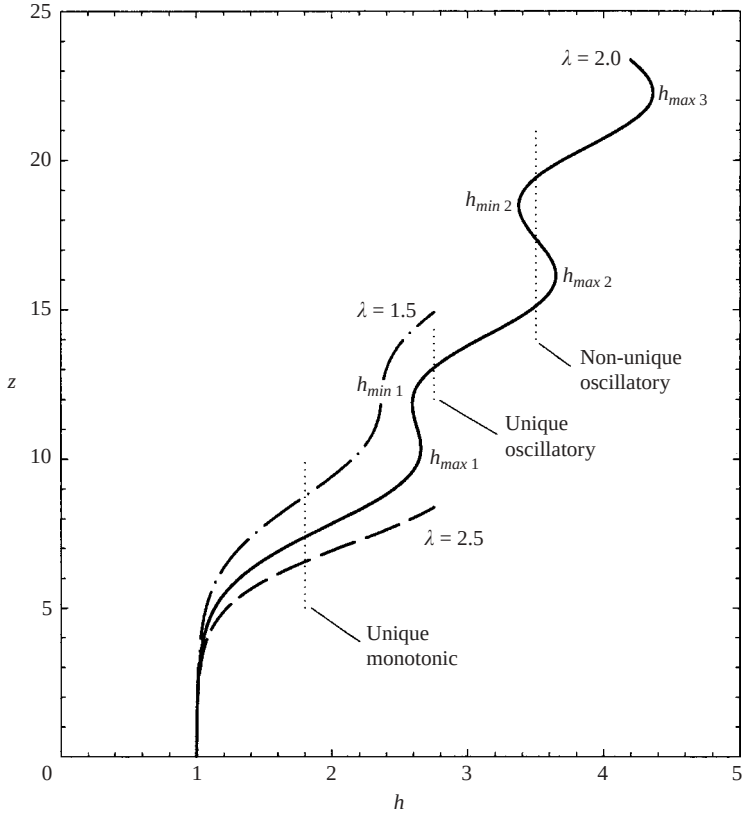

FIGURE 3. Free-surface profiles: monotonic and oscillatory solutions, unique and non-unique examples.

$h = h_i = 3.5$.) When h_i is less than the first local minimum, it is apparent that the solution is always unique (see e.g. $h_i = 2$ in figure 3).

6. Non-unique solutions

By again introducing the translation $\bar{z} = z_0 - z$, it is established in Appendix C that as $\bar{z} \to \infty$

$$h \sim \bar{z}^{1/3}(a + b\cos(\bar{z} - \phi)) + \ldots, \tag{6.1}$$

where

$$a^2 - b^2 = (3\lambda)^{2/3}. \tag{6.2}$$

Since (6.1) implies that $h \gg 1$, the theory is valid only if $\delta h \ll 1$ or equivalently from (2.11), $Ca^{1/3}h \ll 1$. As suggested by (6.1), the values of h at successive maxima ($h_{max\,i}$) increase, as do the values at successive minima ($h_{min\,i}$), see figure 3. For profiles of this type, including at least one local maximum, multiple solutions will arise for all h_i satisfying

$$h_{min\,1} < h_i < h_{max\,1}. \tag{6.3}$$

If, however,

$$h_i < h_{min\,1} \equiv h_{crit}(\lambda) \tag{6.4}$$

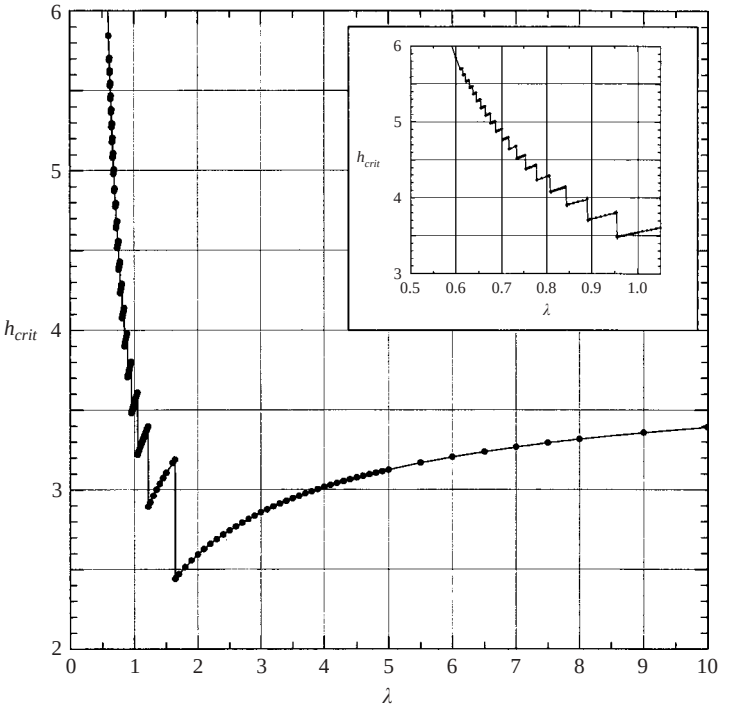

FIGURE 4. Critical thickness for coating flows at small Ca; inset gives an enlarged view for $\lambda < 1$.

the solution will remain unique. As observed in § 5, the solution displayed in figure 3 for $\lambda = 2.0$ is unique when $h_i = 2.50$ and when $h_i = 2.75$, but it is not unique at $h_i = 2.61$. Note that further bands of unique solutions can arise if $h_{min\,2} > h_{max\,1}$, etc.; a detailed discussion of these regimes is not given in this paper.

The function $h_{crit}(\lambda)$, defined by (6.4), is shown in figure 4. It can be seen that the solution is always unique when $h_i < (h_{crit})_{min} \approx 2.43$ for which the corresponding $\lambda \approx 1.64$. When $\lambda > 1.64\ldots$, the numerical calculations indicate that h_{crit} increases monotonically. Asymptotic results for $\lambda \gg 1$ are discussed in § 7. As λ decreases, it appears from figure 4 that transitions in h_{crit} occur at discrete values of λ. An enlarged view of this region is given in the inset to figure 4. These transitions are associated with the merging of the first maximum $h_{max\,1}$ and the first minimum $h_{min\,1}$. A consequence of this collapse is that the first maximum is then equivalent to $h_{max\,2}$. This turning point occurs at an increment in z of one wavelength (approximately 2π), and gives rise to a larger $h_{crit} \equiv h_{min\,2}$.

7. Solutions for large λ

The numerical results in figure 4 suggest that, for large λ, h_{crit} increases monotonically towards an upper bound that is independent of λ. Physically, for a fixed Ca, the limit $\lambda \to \infty$ corresponds to very thin coatings. Note that this limit leads to the classical Landau–Levich solution (§ 4) only when $h_i < h_{crit}$. If $h_i > h_{crit}$, the asymptotic behaviour for $\lambda \gg 1$ requires the matching of solutions that are valid near successive maxima and minima (see figure 3). Determination of this limiting behaviour, together with the structure of the non-unique solution, is described below.

From Appendix A, the eigenvalue for the asymptotic decay $h-1 \sim k\mathrm{e}^{-mz}$ satisfies

$$m^3 + m = \lambda, \tag{7.1}$$

(see (3.5) and (A 2)). Consequently, for $\lambda \gg 1$,

$$m = \lambda^{1/3} - \tfrac{1}{3}\lambda^{-1/3} \ldots, \tag{7.2}$$

which suggests introducing

$$z_0 - z = \lambda^{-1/3}\zeta \tag{7.3}$$

as a new independent variable. Using $z_0(\lambda, h_i)$ as an effective origin for ζ is consistent with the approach discussed in Appendix B. For $h = O(1)$, a suitable local expansion is

$$h = h_0(\zeta) + \lambda^{-2/3}h_1(\zeta) + \ldots. \tag{7.4}$$

It follows from (3.5), (7.3) and (7.4) that

$$h_0^3\frac{\mathrm{d}^3h_0}{\mathrm{d}\zeta^3} = h_0 - 1, \tag{7.5}$$

which is equivalent to the Landau–Levich equation, (4.2). Again, it is required that

$$h_0 - 1 \sim k\mathrm{e}^{\zeta} \tag{7.6}$$

as $\zeta \to -\infty$. As noted in Appendix B, the adoption of a starting value such that $h_0(0) - 1 \ll 1$ (see (7.3)) enables the numerical solution of (7.5) to be obtained. For $\zeta \to \infty\,(z < z_0, \lambda \gg 1)$ the asymptotic growth corresponding to (7.5) is

$$h_0 \sim a_2\zeta^2 + a_1\zeta + a_0 + O(\zeta^{-1}), \tag{7.7}$$

where $a_i(z_0)$ can be found numerically. Note that a_2 is independent of z_0.

Similarly, the first-order term in (7.4) satisfies

$$h_0^3\frac{\mathrm{d}^3h_1}{\mathrm{d}\zeta^3} + \left(2 - 3h_0^{-1}\right)h_1 = -h_0^3\frac{\mathrm{d}h_0}{\mathrm{d}\zeta}, \tag{7.8}$$

for which the decaying solution is required as $\zeta \to -\infty$. In this limit,

$$h_1 \sim -\frac{k}{3}\zeta\mathrm{e}^{\zeta} \tag{7.9}$$

and, strictly, the expansion (7.4) is not uniformly valid. A correction, which can easily be obtained, is required in the region $\zeta = O(\lambda^{2/3})$ where

$$h - 1 \sim k\exp\left(-\tfrac{1}{3}\lambda^{-2/3}\zeta\right)\exp\zeta. \tag{7.10}$$

Of more interest is the behaviour of h_1 as $\zeta \to \infty$. From (7.8) and (7.7), it can be established that

$$h_1 \sim -\tfrac{1}{12}a_2\zeta^4 - \tfrac{1}{6}a_1\zeta^3 + a_{12}\zeta^2 + \ldots, \tag{7.11}$$

where $a_{12}(z_0)$ can be found from the numerical solution of (7.8). Inspection of (7.7) and (7.11) indicates that the expansion fails when

$$\zeta = O\left(\lambda^{1/3}\right) \quad \text{or} \quad z_0 - z = \eta = O(1). \tag{7.12}$$

In this region, which includes the first turning point h_{max1} (see figure 3), $h = O(\lambda^{2/3})$. Setting

$$h = \lambda^{2/3}H(\eta;\lambda) \tag{7.13}$$

leads to the matching condition

$$H \sim a_2\left(\eta^2 - \tfrac{1}{12}\eta^4 + \ldots\right) + \lambda^{-1/3}a_1\left(\eta - \tfrac{1}{6}\eta^3 \ldots\right) + \lambda^{-2/3}\left(a_0 + a_{12}\eta^2 + \ldots\right) + \ldots \quad (7.14)$$

as $\eta \to 0$.

From (3.5), (7.12) and (7.13), it can be seen that $H(\eta;\lambda)$ satisfies

$$H^3\left(\frac{\mathrm{d}^3 H}{\mathrm{d}\eta^3} + \frac{\mathrm{d}H}{\mathrm{d}\eta}\right) = \lambda^{-1}\left(H - \lambda^{-2/3}\right) \quad (7.15)$$

and, from (7.14), a suitable local expansion has the form

$$H = H_0(\eta) + \lambda^{-1/3}H_1(\eta) + \lambda^{-2/3}H_2(\eta) + \ldots. \quad (7.16)$$

Clearly,

$$H_i''' + H_i' = 0 \quad (i = 0, 1, 2). \quad (7.17)$$

After matching with (7.14), the solutions can be written

$$H_0 = 2a_2(1 - \cos\eta), \quad (7.18a)$$

$$H_1 = a_1 \sin\eta, \quad (7.18b)$$

$$H_2 = a_0 + 2a_{12}(1 - \cos\eta). \quad (7.18c)$$

This expansion obviously fails as $\eta \to 2\pi$, where a suitable local independent variable is

$$\eta = 2\pi + \lambda^{-1/3}\hat{\xi}, \quad (7.19)$$

with

$$h = \hat{h}(\hat{\xi};\lambda). \quad (7.20)$$

The structure defined by (7.19) and (7.20) is associated with a region that includes the minimum $h_{min\,1}$ (see figure 3). An immediate similarity with (7.3) and (7.4) is apparent. At leading order in this region, (3.5) also reduces to the Landau–Levich equation

$$\hat{h}^3\frac{\mathrm{d}^3\hat{h}}{\mathrm{d}\hat{\xi}^3} = \hat{h} - 1, \quad (7.21)$$

but now, in contrast with the asymptotic decay (7.6),

$$\hat{h} \sim a_2\hat{\xi}^2 + a_1\hat{\xi} + a_0 + \ldots \quad \text{as} \quad \hat{\xi} \to -\infty. \quad (7.22)$$

The solution of (7.21), subject to (7.22), passes through the local minimum $h_{min\,1}$. As $\hat{\xi} \to +\infty$, however, the asymptotic growth is still of the form (7.7) with a_i replaced by $\hat{a}_i$. Clearly, a periodic structure of the form (7.18) again emerges. This pattern, governed by (7.21), repeats with the coefficients in the algebraic growth laws being dependent on the particular cycle.

As defined in (6.4), h_{crit} corresponds to the first local minimum $h_{min\,1}$. To leading order, the location and magnitude of this minimum are governed by (7.21) and (7.22). In general,

$$\hat{h}(\hat{\xi};\lambda) = \hat{h}_0(\hat{\xi}) + \lambda^{-2/3}\hat{h}_1(\hat{\xi}) + \ldots, \quad (7.23)$$

where $\hat{h}_0$ satisfies (7.21) subject to (7.22). Based on (7.18) and (7.19), it can be established that

$$\hat{h}_1 \sim -\tfrac{1}{12}a_2\hat{\xi}^4 - \tfrac{1}{6}a_1\hat{\xi}^3 + a_{12}\hat{\xi}^2 + \ldots \quad \text{as} \quad \hat{\xi} \to -\infty, \quad (7.24)$$

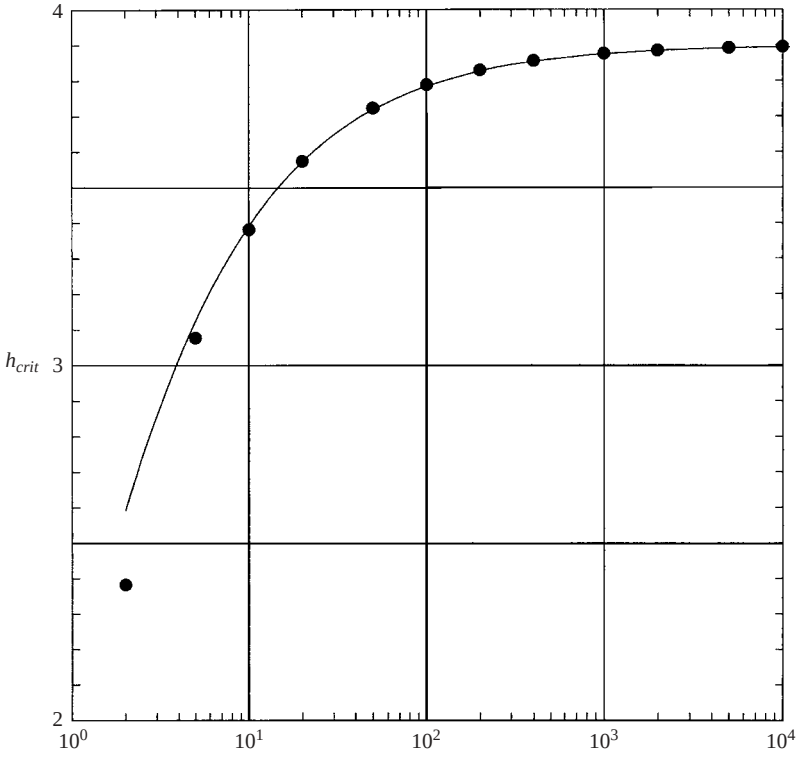

FIGURE 5. Comparison of ——, exact and ●, asymptotic solutions, $\lambda \gg 1$.

and $\hat{h}_1(\hat{\zeta})$ satisfies (7.8). If $\hat{\zeta}_m(\lambda)$ denotes the exact location of the minimum and $\hat{\zeta}_0$ corresponds to the minimum of $\hat{h}_0$, then $\hat{\zeta}_m - \hat{\zeta}_0 = O(\lambda^{-2/3})$ and

$$h_{crit} = \hat{h}(\hat{\zeta}_m; \lambda) = \hat{h}_0(\hat{\zeta}_0) + \lambda^{-2/3}\hat{h}_1(\hat{\zeta}_0) + \ldots, \tag{7.25}$$

since $\hat{h}_0'(\hat{\zeta}_0) = 0$. Numerical solutions of (7.21) and (7.8), employing the matching conditions (7.22) and (7.24), yield

$$h_{crit} \approx 3.900 - 2.53\lambda^{-2/3} + \ldots. \tag{7.26}$$

A comparison with numerical solutions of the full equation (3.5) is shown in figure 5. As can be seen, excellent agreement is obtained for all values of $\lambda > 10$.

As observed at the start of this section, the Landau–Levich theory (§ 4) corresponds to the unique stationary solution when $\lambda \gg 1$ only if $h_i < h_{crit}$.

8. Cylindrical applicators: an illustrative example

In principle, the relationship between the volume flux Q and the applied pressure gradient can be determined for a known applicator geometry. Middleman (1998) presents specific results for a long cylindrical applicator of length L' and constant radius R_0'. For fully developed flow in the applicator, it can be established that

$$h_i\left(1 - K_2 h_i^2\right) = 2, \tag{8.1}$$

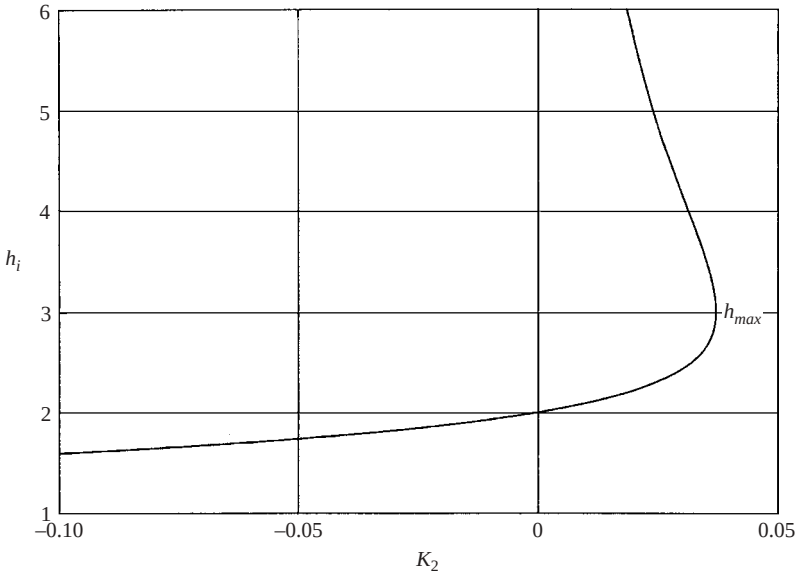

FIGURE 6. Applicator gap for a given pressure gradient.

where

$$K_2 = \tfrac{1}{6}\delta^2 \frac{(p'_e - p'_s)R'^2_f}{\mu L' W'} = -\frac{p_s}{6Ca_3 L}. \tag{8.2}$$

Here, the dimensionless pressure

$$p_s = \frac{p'_s - p'_e}{\sigma / R'_f}, \tag{8.3}$$

where p'_e and p'_s are the applicator exit and supply pressures, respectively. Also, the dimensionless applicator length

$$L = \delta L' / R'_f. \tag{8.4}$$

Note that K_2, and hence (8.1), is independent of the surface tension and corresponds to the ratio between the force due to the applied pressure and the drag exerted on the applicator by the fibre motion. Similarly, it can be shown that the velocity profile within the applicator (narrow gap) can be written

$$w = 1 - \frac{s}{h_i} - 3K_2 s(h_i - s), \tag{8.5}$$

where the radial coordinate s is defined by (2.1) with $0 \leqslant s \leqslant h_i$.

As noted in § 4, when K_2 is small, $h_i \approx 2$. In general, solutions of (8.1) exist only if (see figure 6)

$$K_2 < \tfrac{1}{27}. \tag{8.6}$$

In the range $0 < K_2 < 1/27$, there are two positive solutions of (8.1). For the lower branch, $h < h_m\,(= 3)$, all solutions satisfy

$$3K_2 h_i^2 < 1. \tag{8.7}$$

If $K_2 > 0$, then on the lower branch $2 < h_i < 3$ and the condition (8.7) implies from (8.5) that flow reversal in the applicator will not occur. Note, however, that non-unique

solutions can still arise (see figure 4). On the upper branch, $h > h_m$, all solutions are such that $3K_2h_i^2 > 1$ and flow reversal in the applicator will always occur; again non-unique solutions can arise for certain λ. When $K_2 < 0$, i.e. a strongly pressurized applicator, (8.1) has a single real positive solution, $h_i < 2$ (see figure 6). In this case, reversed flow does not arise and all solutions are unique. Flows with strong adverse pressure gradients, in which $K_2 > 0$, are not expected to arise in practical fibre-coating applications, but the results are included here to provide a full description of the possible range of behaviours.

In the free-surface region, using (3.2) and (3.5), the velocity distribution (3.1) can be expressed as

$$w = 1 - \frac{3(h-1)}{2h}\frac{s}{h}\left(2 - \frac{s}{h}\right), \tag{8.8}$$

where $0 \leqslant s \leqslant h$. Consequently, reversed flow will also take place in the coating if $h > 3\,(= h_m)$. When $h_i < 3$, it may appear that there will be no flow reversal, but the oscillatory results described in § 6 indicate that local solutions with $h > 3$ can still arise. Even if $h_i < 3$, non-unique solutions are possible (see figure 4) provided that $h_i > 2.43\ldots$.

9. Stability issues

Flows of the type considered here are known to be susceptible to Rayleigh instabilities and, in particular, Kalliadasis & Chang have examined such nonlinear instabilities for thin fibre coatings. Similarly, Oron *et al.* have analysed a broad range of time-dependent problems that arise in the physics of thin films. For the configuration discussed in this paper, it can be shown that the unsteady form of (3.5) is

$$\frac{\partial h}{\partial t} + \frac{\partial h}{\partial z} + \lambda^{-1}\frac{\partial}{\partial z}\left(h^3\left(\frac{\partial h}{\partial z} + \frac{\partial^3 h}{\partial z^3}\right)\right) = 0, \tag{9.1}$$

where the time t is made dimensionless using R_f'/W'. With respect to the asymptotic state $h = 1\,(z \to \infty)$, standard linear stability arguments using (9.1) indicate that the flows are unstable, and that the time scale for the maximum growth rate is given by (Hammond 1983)

$$t_g' = 4\lambda\frac{R_f'}{W'}. \tag{9.2}$$

This scale should be compared with a characteristic transit time for a particle leaving the applicator to approach the final state $h = 1$. Based on the asymptotic decay law discussed in Appendix A, one measure for this transit time is

$$t_{tr}' = z_{tr}\frac{R_f'}{W'} = m^{-1}\frac{R_f'}{W'}, \tag{9.3}$$

so that

$$\frac{t_g'}{t_{tr}'} = 4\lambda m. \tag{9.4}$$

As observed in § 1, the liquid coating is solidified by employing a curing process. In practice, the curing station must be located at a distance downstream of the die exit defined by the transit time t_{tr}', i.e. by the length scale $z_{tr}'\,(= m^{-1}R_f'/W')$. For $\lambda \gg 1$

(see A 2)

$$\frac{t_g'}{t_{tr}'} \sim 4\lambda^{2/3} \gg 1 \tag{9.5}$$

and disturbances will not have sufficient time to develop prior to curing. Alternatively, for $\lambda \ll 1$,

$$\frac{t_g'}{t_{tr}'} \sim 4\lambda^2 \ll 1 \tag{9.6}$$

and instabilities can arise before curing. Even for $\lambda > 2$, however, the time-scale ratio is greater than eight, and curing should occur before surface instabilities dominate.

10. Summary

In the lubrication limit, classical coating theory at small capillary numbers leads to the Landau–Levich equation, (4.2), in which axial curvature dominates; that analysis is valid when the dimensionless thickness $\delta = O(Ca^{2/3})$. For larger die gaps, i.e. larger coating thicknesses, the classical approach fails. This paper provides an analysis for the limit when $\delta = O(Ca^{1/3})$. As noted earlier, some experimental results for dip-coating (Darhuber *et al.* 2000) are in accord with the latter scaling in which the Landau–Levich equation for the free-surface profile is replaced by (3.5) for which both axial and circumferential curvatures are important. Coating flows corresponding to the oscillatory behaviours described here were not discussed in Darhuber *et al.*

Solutions of (3.5) are dependent on the dimensionless group $\lambda = 3Ca\delta^{-3}$ and the dimensionless die gap h_i. Numerical calculations indicate that this equation has a unique solution for all λ provided that $h_i < 2.43\ldots$. At larger values of h_i, the numerical results demonstrate the possible existence of free-surface spatial oscillations, and the time-independent solution is not necessarily unique. A band of non-unique solutions first arises in the interval

$$h_{min1} < h_i < h_{max1}, \tag{10.1}$$

and the critical gap $h_{crit} \equiv h_{min\,1}$. Computations of the critical gap size $h_{crit}(\lambda)$ illustrate that discontinuities in this function occur at discrete values of λ. Knowledge of h_{crit} provides an important constraint on die geometry. Exceeding h_{crit} can generate spatial surface oscillations that may prevent the production of a uniform coating thickness. It was recognized in § 6, however, that for $h > h_{crit}$ unique solutions can still exist in restricted regions of the parameter space.

Appendix A. Asymptotic decay

As $h \to 1$, it follows from (3.5) that

$$h - 1 \sim k\mathrm{e}^{-mz}, \tag{A 1}$$

and the eigenvalue m satisfies

$$m^3 + m = \lambda, \tag{A 2}$$

where λ is defined by (3.7) and (2.11).

Since $\lambda > 0$, (A 2) has a single real positive solution together with a complex conjugate pair. The sum of the roots of (A 2) is zero so that the real part of the conjugate pair is negative. Only the real positive eigenvalue is acceptable, and the requirement (2.3) imposes two constraints on the solution of (3.5).

Appendix B. Computational procedure

As noted earlier, the imposition of (2.3) eliminates two growing solutions of (3.5). Consequently, the limiting behaviour as $z \to \infty$ has the form

$$h - 1 \sim b_1 \mathrm{e}^{-mz} + \ldots, \tag{B 1}$$

where m is the real positive root of (A 2).

Since (3.5) is invariant under translation with respect to z, it is convenient to rewrite (B 1) as

$$h - 1 \sim \bar{b}_1 \mathrm{e}^{m\bar{z}} + \ldots, \tag{B 2}$$

where

$$\bar{z} = z_0 - z, \quad \bar{b}_1 = b_1 \exp(-mz_0). \tag{B 3}$$

It is now permissible to identify $\bar{b}_1$ by choosing

$$h - 1 \equiv \bar{h} = \bar{h}_b \ll 1 \quad \text{at} \quad \bar{z} = 0. \tag{B 4}$$

Imposing the requirement that $\bar{h} \to 0$ as $\bar{z} \to -\infty$, leads to the asymptotic representation

$$\frac{\mathrm{d}\bar{h}}{\mathrm{d}\bar{z}} \sim m\bar{h} + m_2\bar{h}^2 + \ldots, \quad \frac{\mathrm{d}^2\bar{h}}{\mathrm{d}\bar{z}^2} \sim m^2\bar{h} + 3mm_2\bar{h}^2 + \ldots, \tag{B 5}$$

with

$$m_2 = -3\lambda/(7m^2 + 1), \text{ etc.} \tag{B 6}$$

These results for the first and second derivatives can be used to initiate the numerical calculation starting at $\bar{z} = 0$ with $\bar{h} = \bar{h}_b$. Backward integration enables the parameter z_0 to be identified by the value of $\bar{z}$ at which $h = h_i$, where $z = 0$. The profile for $h = h(z; h_i)$ then follows.

Appendix C. Behaviour for large h_i

Using the translation $\bar{z} = z_0 - z$, inspection of (3.5) suggests that the dominant approximation as $\bar{z} \to \infty$ ($h_i \gg 1$) has the form

$$h \sim \bar{z}^{-1/3} f(\bar{z}), \tag{C 1}$$

where $f(\bar{z})$ satisfies

$$f''' + f' \approx 0,$$

so that

$$f(\bar{z}) \sim a_0 + b_0 \cos\bar{z} + c_0 \sin\bar{z}. \tag{C 2}$$

Note that, although $h_i \gg 1$, it is necessary that $\delta h_i \ll 1$ for the thin-film assumption to be valid. Inspection of higher-order terms indicates that, in general, secular behaviours can occur over length scales $O(h_i^3)$ and justification of (C 1) and (C 2) requires a more careful analysis that is given below.

The secular behaviour indicates that it is necessary to carry out a multiple scales analysis by introducing

$$Y = \varepsilon\bar{z}, \quad \bar{y} = (1 + o(\varepsilon))\bar{z}, \tag{C 3}$$

where

$$\varepsilon = h_i^{-3}. \tag{C 4}$$

It is now appropriate to set

$$h = h_i F(\bar{y}, Y; \varepsilon), \tag{C 5}$$

where no assumption concerning the functional form of $F(\bar{y}, Y; \varepsilon)$ is made. Using (C 3)–(C 5), (3.5) becomes

$$F^3\left[\frac{\partial^3 F}{\partial \bar{y}^3} + \frac{\partial F}{\partial \bar{y}} + \varepsilon\left(3\frac{\partial^3 F}{\partial \bar{y}^2 \partial Y} + \frac{\partial F}{\partial Y}\right) + O(\varepsilon^2)\right] = \varepsilon\lambda F + O\left(\varepsilon^{4/3}\right). \tag{C 6}$$

Consistent with (C 6), $F(\bar{y}, Y; \varepsilon)$ can be expanded in the form

$$F = F_0(\bar{y}, Y) + \varepsilon F_1(\bar{y}, Y) + \ldots, \tag{C 7}$$

which leads to

$$\frac{\partial^3 F_0}{\partial \bar{y}^3} + \frac{\partial F_0}{\partial \bar{y}} = 0,$$

or

$$F_0 = A_0(Y) + B_0(Y)\cos\bar{y} + C_0(Y)\sin\bar{y}. \tag{C 8}$$

Similarly, F_1 satisfies

$$\frac{\partial^3 F_1}{\partial \bar{y}^3} + \frac{\partial F_1}{\partial \bar{y}} = \frac{\lambda}{F_0^2} - \frac{\mathrm{d}A_0}{\mathrm{d}Y} + 2\frac{\mathrm{d}B_0}{\mathrm{d}Y}\cos\bar{y} + 2\frac{\mathrm{d}C_0}{\mathrm{d}Y}\sin\bar{y} = R_1(\bar{y}, Y). \tag{C 9}$$

Possible secular growth is eliminated by using the orthogonality requirements

$$\int_0^{2\pi} R_1(\bar{y}, Y)\{1, \cos\bar{y}, \sin\bar{y}\}^T \mathrm{d}\bar{y} = 0. \tag{C 10}$$

From (C 9) and (C 10), using Gradshteyn & Ryzhik (1994), it can be established that

$$\frac{\mathrm{d}M_i}{\mathrm{d}Y} = \frac{\lambda M_i}{\left(A_0^2 - B_0^2 - C_0^2\right)^{3/2}}, \tag{C 11}$$

where $M_i = A_0$, B_0 or C_0. Consequently, the asymptotic behaviour is described by

$$A_0 = a_0 Y^{1/3}, \quad B_0 = b_0 Y^{1/3}, \quad C_0 = c_0 Y^{1/3}, \tag{C 12}$$

with

$$a_0^2 - b_0^2 - c_0^2 = (3\lambda)^{2/3}. \tag{C 13}$$

Note that (C 8) and (C 12) still imply that the asymptotic behaviour has the form (C 2), but now the coefficients are related through (C 13).

Writing

$$a_0 = a, \quad b_0 = b\cos\phi, \quad c_0 = b\sin\phi, \tag{C 14}$$

gives the limiting result (6.1), i.e.

$$h \sim \bar{z}^{-1/3}(a + b\cos(\bar{z} - \phi)), \tag{C 15}$$

where

$$a^2 - b^2 = (3\lambda)^{2/3}. \tag{C 16}$$

REFERENCES

Batchelor, G. K. 1967 *An Introduction to Fluid Dynamics*, p. 220. Cambridge University Press.

Benjamin, D. F. & Scriven, L. E. 1991 Coating flows: form and function. *Ind. Coating Res.* **1**, 1–37.

Blythe, P. A. & Simpkins, P. G. 1995 Fiber coating thickness predictions at low capillary numbers. *Bull. Am. Phys. Soc.* **40**, 2016.

Bretherton, F. P. 1961 The motion of long bubbles in tubes. *J. Fluid Mech.* **10**, 166–188.

Darhuber, A. A., Troian, S. M., Davis, J. M. & Miller, S. M. 2000 Selective dip-coating of chemically micropatterned surfaces. *J. Appl. Phys.* **88**, 5119–5126.

Eggers, J. 1997 Nonlinear dynamics and the breakup of free-surface flows. *Rev. Mod. Phys.* **69**, 865–929.

Finn, R. 1986 *Equilibrium Capillary Surfaces*. Springer.

Frenkel, A. L. 1992 Nonlinear theory of strong undulating thin films flowing down vertical cylinders. *Europhys. Lett.* **18**, 583–588.

de Gennes, P. G. 1985 Wetting: statics and dynamics. *Rev. Mod. Phys.* **57**, 827–863.

Gradshteyn, I. S. & Ryzhik, I. M. 1994 *Tables of Integrals, Series and Products*, 5th edn, p. 182. Academic.

Hammond, P. S. 1983 Nonlinear adjustment of a thin annular film of viscous fluid surrounding a thread of another within a circular cylindrical pipe. *J. Fluid Mech.* **137**, 363–384.

Jensen, O. E. 1997 The thin liquid lining of a weakly curved cylindrical tube. *J. Fluid Mech.* **331**, 373–403.

Kalliadasis, S. & Chang, H.-C. 1994 Drop formation during coating of vertical fibers. *J. Fluid Mech.* **261**, 135–168.

Landau, L. & Levich, B. 1942 Dragging of a liquid by a moving plate. *Acta Physiochim. USSR* **17**, 42–54.

Middleman, S. 1995 *Modeling of Axisymmetric Flows*. Academic.

Middleman, S. 1998 *An Introduction to Fluid Dynamics*. John Wiley.

Myers, T. 1998 Thin films with high surface tension. *SIAM Rev.* **40** (8).

Oron, A., Davis, S. H. & Bankoff, S. G. 1997 Long-scale evolution of thin liquid films. *Rev. Mod. Phys.* **69**, 931–980.

Quéré, D. 1990 Thin films flowing on vertical fibers. *Europhys. Lett.* **13**, 721–726.

Quéré, D. 1999 Fluid coating on a fiber. *Annu. Rev. Fluid Mech.* **31**, 347–384.

Ruschak, K. J. Coating flows. 1985 *Annu. Rev. Fluid Mech.* **17**, 65–89.

de Ryck, A. & Quéré, D. 1996 Inertial coating flows. *J. Fluid Mech.* **311**, 219–337.

Tuck, E. O. & Schwartz, L. W. 1990 A numerical and asymptotic study of some third order ordinary differential equations relevant to draining and coating flows. *SIAM Rev.* **32**, 453–469.

Weiss, P. 1999 To bead or not to bead? *Sci. News* **155**, 28–30.